Structure-sensitivity of alumina supported palladium catalysts for N_2O decomposition

Nia Richards[1], James H. Carter[1], Ewa Nowicka[1], Luke A. Parker[2], Samuel Pattisson[1], Qian He[1], Nicholas F. Dummer[1], Stanislaw Golunski[1], Graham J. Hutchings[1]*

[1]Cardiff Catalysis Institute, School of Chemistry, Cardiff University, Cardiff, CF10 3AT UK

[2]Now at; Inorganic Chemistry and Catalysis Debye Institute for Nanomaterials Science, Utrecht University, Universiteitsweg 99, 3584CG Utrecht (The Netherlands)

*Corresponding author: Hutch@cardiff.ac.uk

Abstract

The catalytic activity of $Pd/\gamma Al_2O_3$ for N_2O decomposition was found to be highly dependent on the preparation methodology and the number of reaction cycles. Chloride species on the surface of a 2.6 wt. % $Pd\text{-}Al_2O_3$ catalyst prepared by wet impregnation were identified as inhibiting the activity. Multiple reaction cycles were shown to remove these species, and a subsequent increase in activity was observed; 10.3 $mol_{N2O}\ h^{-1}\ kg_{cat}^{-1}$ in the first use, increased to 28.7 $mol_{N2O}\ h^{-1}\ kg_{cat}^{-1}$ on the fourth use both at 550 °C. Additionally, removal of physisorbed water from the support prior to metal deposition increased the thermal stability of Pd nanoparticles and increased the catalyst activity. Catalysts were subsequently prepared using a deposition technique with an increased concentration of Cl^- ions resulted in increased Pd-Cl species in the final catalyst and the catalytic activity was consequently increased due to the improved control of Pd particle size.

Keywords: Nitrous Oxide Decomposition, Particle Size, CO Chemisorption, HAADF-STEM, $Pd\text{-}Al_2O_3$.

1 Introduction

Nitrous oxide (N_2O) is a highly potent greenhouse gas, this being evidenced by its global warming potential of *ca.* 300 relative to CO_2 [1–3]. 60 % of the global N_2O emissions are anthropogenic and include industrial chemical processes, sewage treatment, combustion sources (both stationary and mobile) and the agricultural sector [4–7], while adipic acid production accounts for around 80 % of the global industrial emission of N_2O [6,8]. There are also small industrial uses such as hospital and dental surgeries [9]. Consequently, it is of great importance to develop catalysts that can efficiently decompose N_2O (Eq. 1):

$$\mathbf{2\ N_2O \rightarrow 2\ N_2 + O_2} \qquad (\Delta_r H^o\ (298\ K) = -163\ kJmol^{-1})\ [10] \qquad \text{(Eq. 1)}$$

There are many catalysts that can be used for N_2O decomposition including perovskites [11–15], ceria-based catalysts [16–18], spinels [19–21] and supported metal catalysts [22–26]. This work focuses on palladium/alumina (Pd-Al_2O_3) catalysts as these have not been extensively studied to date [27–31] and similar catalytic systems have been demonstrated to exhibit high activity and stability in similar applications [32–37]. Pekridis *et al.* reported a T_{100} (i.e. the temperature to reach 100 % conversion) of 425 °C using a 2 wt. % Pd-Al_2O_3 catalyst prepared by wet-impregnation. They also showed that the addition of propane to the gas feed lowered the T_{100} to 400 °C [27]. The rate-limiting step in the decomposition of N_2O is typically the recombination of oxygen to form O_2 [38–44] and propane acts as reductant that can facilitate the abstraction of oxygen from the oxidised active site, significantly increasing the observed rate of N_2O decomposition at lower temperatures [27,28]. In addition to propane [45–49] ethane, methane and CO [49–54] have also been used as reductants. Christoforou *et al.* reported that 72 % conversion was possible using 2 wt. % Pd-Al_2O_3 at 600 °C, the addition of propane to the feed lowers the temperature required for 100 % conversion by over 200 °C. [28]. Doi *et al.* utilised a higher weight loading of 5 % with only 60 ppm N_2O in the gas stream and showed that it was possible to decompose this low concentration of N_2O at 300 °C; however, air was used as the balance gas of this reaction and in this case that the addition of oxygen to the feed increases the activity [31]. It is important to note that in most cases the addition of oxygen to the gas feed limits the conversion of N_2O, this is because the oxygen present oxidises the active site of the catalysts [22,27,55].

A range of Pd concentrations have been shown to be active for the decomposition of N_2O. Tzitzios *et al.* prepared a 0.5 wt.% Pd- Al_2O_3 catalyst by wet impregnation using a nitrate precursor that achieved 55 % conversion of N_2O at 550 °C. The group showed that the presence of a reductant (CO) to the feed lowers the temperature required for 50 % conversion (T_{50}) from 536 °C to 366 °C, a decrease of 170 °C in the operating temperature.[56] Parres-Esclapez *et al*. also prepared a 0.5 wt.% Pd-Al_2O_3 catalyst by

impregnation using a Pd acetate precursor that converted 34 % N_2O present at 600 °C.[22] Staying on the theme of low Pd loadings, Pachatouridou *et al.* prepared a 1 wt.% Pd-Al_2O_3 catalyst by dry impregnation, that reached 78 % conversion at 600 °C, with a T_{50} of 525 °C.[57] Tateishi *et al.* demonstrated that a higher weight loading was also good for this reaction with a commercial 5 wt.% Pd-Al_2O_3 catalyst achieving 100 % conversion at 320 °C, but the catalyst that the group prepared by wet impregnation required 500 °C to achieve the same conversion in the same conditions (noting O_2 present in gas feed) [30].

In this work, we investigate the importance of surface species and particle size of Pd-Al_2O_3 catalysts for the decomposition of N_2O in the presence and absence of a reductant, propane. The effect of removing surface species such as water and chloride ions have been investigated by different pre-treatments and support pre-treatments. In addition to comparing how activity changes based on these pre-treatments, we have evaluated how the surface sensitivity of these catalysts can be used to control the particle size and consequently, catalyst activity. Through pre-treatment of the catalyst support prior to the metal deposition, the catalytic activity is significantly increased, resulting in a decrease of the N_2O T_{100} by 150 °C to 400 °C, in the presence of propane.

2 Experimental

2.1 Catalyst Preparation

2.6 wt.% Pd-Al_2O_3 was prepared by wet impregnation as described by Pekridis *et al*. [27], $PdCl_2$ was dissolved in deionised water to give a solution with a concentration of 6 mg mL^{-1}. γ-Al_2O_3 (0.98 g, Sigma Aldrich, average particle size < 50 nm) was then added to the solution (4.6 mL) and heated slowly to 55 °C with stirring to remove the water via evaporation until a slurry was formed. The slurry was then dried in an oven at (120 °C, 2 h) and calcined (600 °C, 4 h, heating rate 10 °C min^{-1} in flowing air). Where stated further heat treatments were carried out at 600 °C for 1 h at 20 °C min^{-1} in flowing air. In some cases γ-Al_2O_3 was calcined before catalyst preparation at 600 °C for 4 h at 10 °C min^{-1} in flowing compressed dry air. The following denominations were assigned to various catalysts: **SC** – Support calcined at 600 °C for 4 h at 10 °C min^{-1} in flowing compressed dry air before catalyst preparation. **5HT** – catalyst prepared, calcined and subjected to 5 more heat treatments at 600 °C for 1 h at 20 °C min^{-1} in flowing compressed dry air. **4R** – catalyst that has been through four reaction cycles. **5R** – catalyst that has been through five reaction cycles.

2.1 wt.% Pd-Al_2O_3 was prepared by a modified impregnation method as described by Morad and co-workers [58]. $PdCl_2$ was dissolved in water to give a solution with a concentration of 6 mg mL^{-1}, HCl was added to acidify the solution until a concentration of 0.58 M was achieved. De-ionised water was added to the solution (3.49 mL) to a total volume of 16 mL in a 50 mL round bottom flask. The solution was heated to 60 °C in an oil bath. γ-Al_2O_3 (0.98 g, Sigma Aldrich, average particle size < 50 nm) was added to the solution slowly over a period of 10 min. The slurry was left to stir for 15 min and then the temperature was increased to 95 °C and left to dry for 16 h. The resulting solid was calcined at 600 °C for 4 h at 10 °C min^{-1} in flowing compressed dry air. As with the wet impregnation samples, one catalyst was prepared with γ-Al_2O_3 that had been calcined before catalyst preparation at 600 °C for 4 h at 10 °C min^{-1} in flowing compressed dry air and was also denoted support calcined (**MI SC**). The catalyst that was prepared by modified impregnation using untreated Al_2O_3 was denoted **MI**.

2.2 N_2O decomposition studies

All reactions were performed at atmospheric pressure in a continuous-flow fixed-bed reactor. A reactor tube (4.6 mm internal diameter, stainless steel) was packed with catalyst (0.0625 g) between two layers of quartz wool. Reactions were performed over the temperature range of 200 – 600 °C, with a flow rate of 100 ml/min (GHSV 76690 h^{-1}). The gas feed was composed of 1 % N_2O in He or 1 % N_2O and 1 % C_3H_8 in He. All outgoing gaseous products were analysed online using an Agilent 7890B Gas Chromatograph (GC) (columns: Hayesep Q (80-100 mesh, 1.8 m) MolSieve 5A (80-100 mesh, 2 m)

fitted with a thermal conductivity detector. Pre-treatment of the γ-Al_2O_3 in the reactor prior to the addition of the metal was carried out using 13 % O_2 and 87 % N_2 from separate cylinders (BOC grade N4, 99.99 %).

2.3 Catalyst Characterisation

X-ray photoelectron spectroscopy (XPS) was performed on a Thermo Fisher Scientific K-alpha$^+$ spectrometer. Samples were analysed using a micro-focused monochromatic Al X-ray source (72 W) over an area of approximately 400 microns. Data was recorded at pass energies of 150 eV for survey scans and 40 eV for high resolution scan with 1 eV and 0.1 eV step sizes respectively. Charge neutralisation of the sample was achieved using a combination of both low energy electrons and argon ions. Data analysis was performed in CasaXPS using a Shirley type background and Scofield cross sections, with an energy dependence of -0.6.

Solid-state Magic Angle Spinning Nuclear Magnetic Resonance (MAS-NMR) spectra were obtained at the EPSRC UK National Solid-state NMR Service Durham University. Solid state ^{1}H Proton spectra were recorded at 399.88 MHz using a Varian VNMRS spectrometer and a 4 mm (rotor o.d.) magic-angle spinning probe. They were obtained using a background suppression pulse sequence, 128 repetitions with a 1 s recycle delay and a spin-rate of approximately 14 kHz. Spectral referencing was to external, neat tetramethylsilane carried out by setting the resonance from adamantane to 1.9 ppm.

Powder X-Ray Diffraction (XRD) analysis was performed on a PANalytical X'Pert Pro diffractometer using a Ni-filtered CuKα radiation source operating at 40 KV and 40 mA. Standard analysis was performed using a 40 minute run with a back filled sample holder. Patterns were identified using the International Center for Diffraction Data Powder Diffraction File.

In-situ XRD was performed using a PANalytical X'Pert Pro diffractometer using a Ni-filtered CuKα radiation source operating at 40 KV and 40 mA, fitted with a cell that allows temperature control and gas flow using Bronkhorst MFC's. 'Data collector' program controls temperature settings, run time and repeats. Patterns were identified using the International Center for Diffraction Data Powder Diffraction File.

High-Angle Annular Dark-Field Scanning Transmission Electron Microscopy (HAADF-STEM) was performed using a JEOL ARM 200CF AC-STEM instrument and the samples were prepared using the dry dispersion route: The catalyst powder was ground between two clean glass slides and then dry transferred onto a holey carbon TEM grid.

Inductively Coupled Plasma – Optical Emission Spectroscopy (ICP-OES) was performed by Exeter Analytical Services using HF digestion to get an accurate Pd loading. The sample was digested by Anton Paar Multiwave 3000 microwave with nitric and HF acids – then the HF was neutralised with the addition of Boric Acid. A reagent blank was carried out. Internal standard was added to the resulting solutions and the blank and sample were run against Fe standards by ICP-OES using Thermo Fisher iCAP Duo 7400.

CO Chemisorption was performed using a ChemBET TPR/TPD pulsar with a reduction in 10 % H_2/Ar up to 150 °C before carrying out CO chemisorption at room temperature using 10 % CO/He using an attenuation of 2, TCD sensitivity of 150 and CO flow of 15 mL min^{-1}. An automated pulse program was used with a pulse length of 400 seconds, loop volume 125 µL, 16 pulses and a stable baseline.

3 Results and Discussion

Pd-Al_2O_3 catalysts have previously been shown to catalyse N_2O decomposition at high reaction temperatures (>500 °C) [22,27,30,56,57]. Initially, their stability was investigated through the use of multiple reaction cycles. The catalyst was heated step wise from 200 – 600 °C in 50 °C increments under a mixture of N_2O (1 %) in helium and the N_2O conversion was recorded every 50 °C. Following this, the catalyst bed was cooled under flowing helium and the reaction process repeated. In each cycle, the catalyst was exposed to the same pre-treatment as the initial test, as described in the experimental section. The catalytic activity could then be compared across the reaction cycles and differences investigated through material characterisation.

Firstly, a blank reaction was performed with only quartz wool and no catalyst. No conversion of N_2O was measured over the temperature range of 300 – 600 °C, indicating the reactor was not active over the temperature range of interest (Table 1, entry 1). Decomposition of N_2O was studied using 2.6 wt. % Pd-Al_2O_3 prepared by wet impregnation, with a pre-treatment (1 h at 600 °C, 13 % O_2, 87 mL min^{-1}) over the temperature range 300 – 600 °C. The fresh catalyst (Table 1 entry 2) was able to convert 10.3 mol_{N2O} h^{-1} kg_{cat}^{-1} at 550 °C, while the catalyst by Tzitzious *et al*. converted 20.9 mol_{N2O} h^{-1} kg_{cat}^{-1} at the same temperature.[56]

Table 1. The effect of multiple reaction cycles or heat treatments on N_2O conversion over 2.6 wt. % Pd-Al_2O_3 catalysts.

Entry	Catalyst (2.6 wt. % Pd-Al_2O_3)	T_{50}[a] (°C)	Conversion at 550 °C (%)	Decomposition Rate at 550 °C (mol_{N2O} h^{-1} kg_{cat}^{-1})
1	Blank	-	0	0
2	Fresh	577	24	10.3
3	2R	565	39	16.7
4	3R	542	56	24.0
5	4R	527	67	28.7
6	5R	540	57	24.4
7	5HT	584	22	9.4

[a] temperature required for 50 % N_2O conversion;

The catalytic activity was found to increase with each reaction cycle up to the fourth use (Table 1 entries 3-5). After the second reaction cycle the decomposition rate increased from 16.7 to 24.0, this increased to a maximum at the 4th use (4R) 28.7 mol_{N2O} h^{-1} kg_{cat}^{-1}. For the fifth cycle a decrease in the decomposition rate was observed to 24.4 mol_{N2O} h^{-1} kg_{cat}^{-1}. The observed increase in activity after multiple uses was investigated further by replicating the five heat treatment cycles *ex situ*, i.e. in a furnace (flowing air at 600 °C for 1 h) to simulate the reaction conditions. The activity of this catalyst (denoted 5HT) did not compare to that of the multiple use catalyst, but was comparable to the fresh catalyst (Table 1, entry 7 and Fig. 1). The decomposition rate at 550 °C was 9.4 mol_{N2O} h^{-1} kg_{cat}^{-1}.

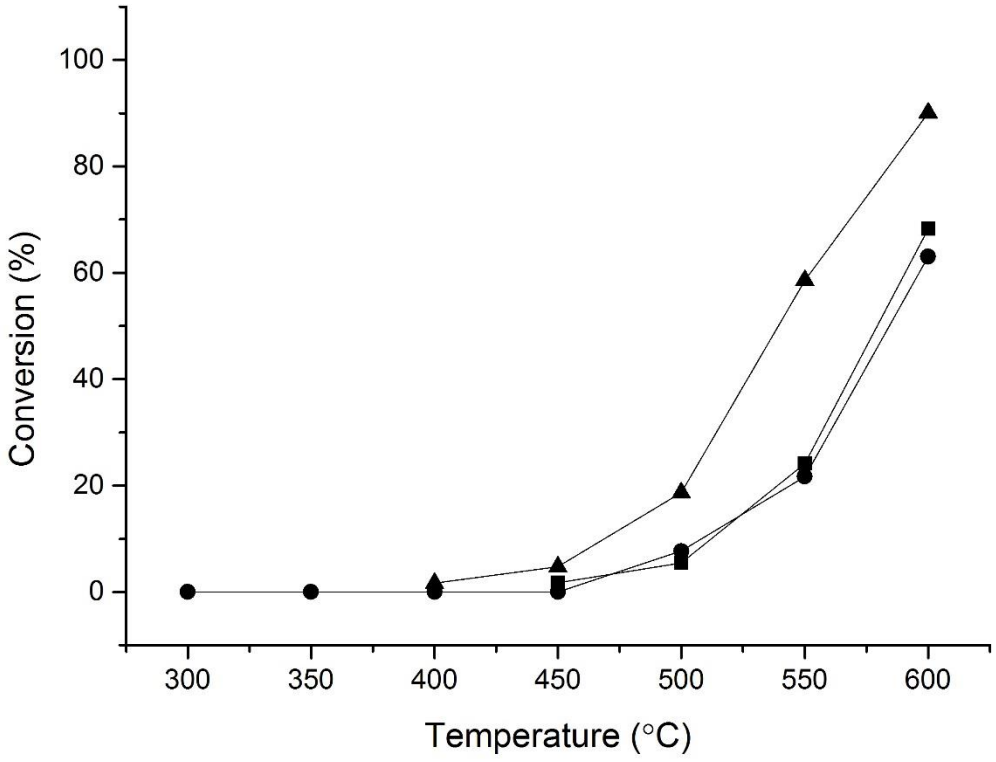

Fig. 1. The effect of multiple uses or heat treatments on N_2O decomposition using a 2.6 wt. % Pd-Al_2O_3 catalyst. Reaction Conditions: 1 % N_2O/He, total flow 100 mL min^{-1}, GHSV: 76690 h^{-1} Legend: ■ - 2.6 wt. % Pd-Al_2O_3 Fresh, ● - 2.6 wt. % Pd-Al_2O_3 **5HT**, ▲- 2.6 wt. % Pd-Al_2O_3 **5R**.

The Pd-Al_2O_3 catalysts were then characterised in an attempt to understand the origin of the activity differences observed over multiple reaction cycles and heat-treatments compared to the fresh sample. The samples of interest were the fresh 2.6 wt. % Pd-Al_2O_3 catalyst, the catalyst after five reaction cycles (**5R**) and the catalyst after five heat-treatments (**5HT**). Fig. 2 illustrates the X-ray diffraction patterns; the support exhibits only alumina reflections, as does the fresh 2.6 wt. % Pd-Al_2O_3 catalyst, reflection are assigned to γ-Al_2O_3 (3 1 1) 2θ = 37.1 °, (4 0 0) 2θ = 46.0 ° and (4 4 0) 2θ = 66.6 ° [59]. There is no reflection present for Pd in the fresh catalyst, which indicates that the particle size of Pd is below the XRD nanoparticle detection limit. In contrast, the **5R** and **5HT** catalysts exhibited reflections due to Pd as PdO (1 0 1) 2θ = 33.855 °, PdO (3 1 1) 2θ = 54.900 ° and PdO (2 1 1) 2θ = 71.485 ° [60]. A Pd^0 reflection was observed at Pd (1 1 1) 2θ = 42.034 ° [61]. In the used (**4R** and **5R**) and **5HT** catalysts there are reflections present due to both PdO and Pd, this presence of reflections suggests that Pd nanoparticles have sintered as the particles are now observable by XRD.

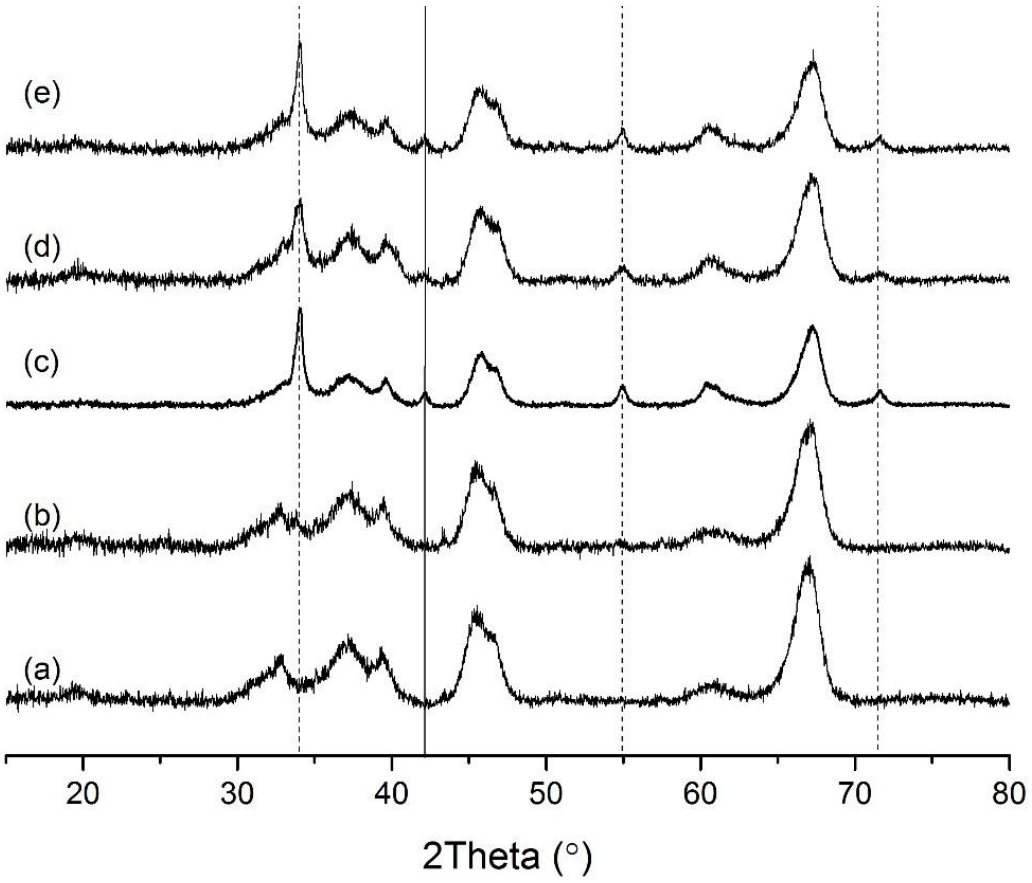

Fig. 2. XRD patterns for γ-Al_2O_3 and 2.6 wt. % Pd-Al_2O_3 catalysts; (a) Al_2O_3 support, (b) 2.6 wt. % Pd-Al_2O_3 Fresh, (c) 2.6 wt. % Pd-Al_2O_3 **4R**, (d) 2.6 wt. % Pd-Al_2O_3 **5R**, (e) 2.6 wt. % Pd-Al_2O_3 **5HT**, dashed line – PdO, solid line – Pd, all unlabelled reflections are due to γ-Al_2O_3.

The improvement in activity on repeated uses may have been caused by the removal of residual Cl species that has been reported to poison the catalyst [62]. This would be achieved over the reaction cycles through a process of converting any remaining Pd-Cl species to PdO. X-Ray photoelectron spectroscopy (XPS) was used to investigate the surface composition and oxidation state of Pd in more detail (Fig. 3). In general, two peaks at 336.8 eV and 334.9 eV are observable in the Pd 3d core level XPS spectra, with the peak at 336.8 eV ascribed to PdO-Al_2O_3 as previously reported by Batista *et al.* [63] while the peak at 334.9 eV can be attributed to Pd^0 on Al_2O_3 [64,65]. Depending on catalyst preparation techniques Pd-Cl species can also be present in the spectra and correspond to the peaks at 338.2 eV [66]. Each Pd species has two peaks assigned to it due to the spin orbit splitting value of 5.3 eV [67,68]. All catalysts show only PdO and Pd-Cl species and the concentration of these species was observed to change as the catalyst was subjected to reaction conditions. Specifically, the proportion of Pd-Cl species decreased while PdO species increased, overall. The **5R** catalyst shows an increase in PdCl species over the **4R** catalysts. This is not because the catalyst has gained Cl, but because the % Pd present has decreased meaning more of the surface of the Pd is in the form PdCl as sintering has taken place. (**Error! Reference source not found.**). When the catalyst was heated in the

furnace (**5HT**) almost all the PdCl species were removed (Fig. 3), however, the catalytic activity is not improved above that of the fresh catalyst. As the number of heat treatments increases the surface concentration of total atomic Pd % (as given by XPS) decreases (Table 2), this indicates that the % of Pd at the surface has decreased, which can indicate Pd sintering or agglomeration has taken place.

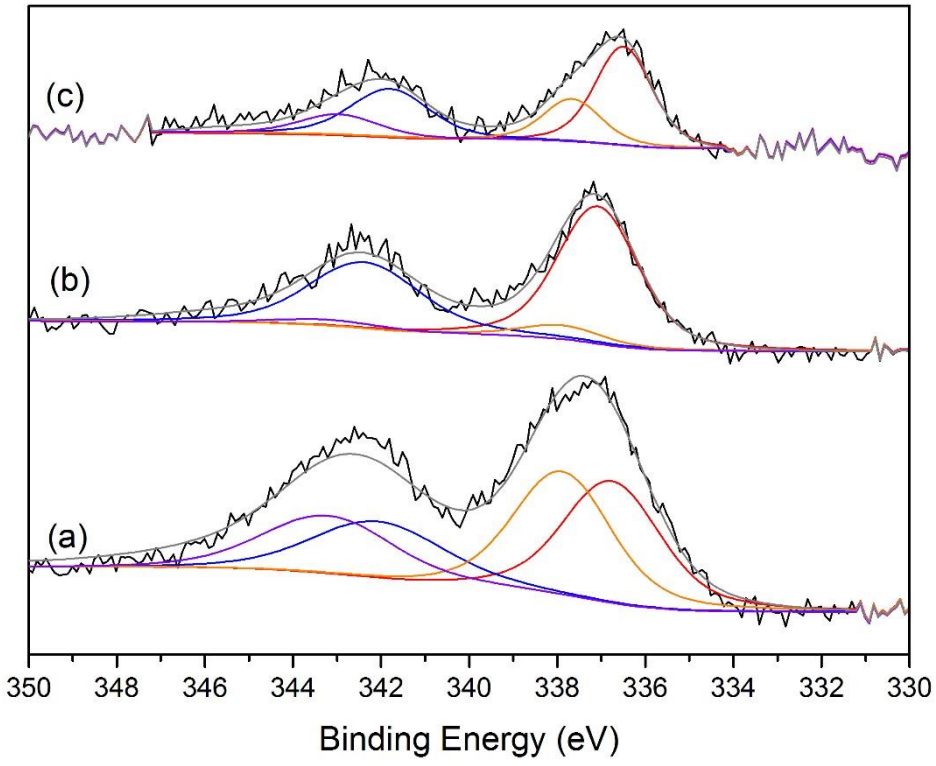

Fig. 3. XPS spectra for various 2.6 wt. % Pd-Al_2O_3 catalysts (a) Fresh, (b) **5HT**, (c) **5R**. Each spectra is fitted with two peaks corresponding to PdO (Red and Blue lines) and Pd-Cl (Orange and Purple species).

Table 2. Surface composition of Pd-Al_2O_3 catalysts as reported by XPS analysis.

Catalyst	Pd 3d (at.%)	% of PdO (337 eV) (%)	% of PdCl (339 eV) (%)
2.6 wt. % Pd-γAl_2O_3 Fresh	0.46	50	50
2.6 wt. % Pd-γAl_2O_3 **4R**	0.40	78	22
2.6 wt. % Pd-γAl_2O_3 **5R**	0.11	72.7	27.3
2.6 wt. % Pd-γAl_2O_3 **5HT**	0.25	92	8

The XRD patterns indicate that with increased reaction cycles and heat treatments Pd sintering took place. Furthermore, XPS measurements indicated that in addition to sintering the population of Pd-Cl species decreased across the samples. However, the N_2O decomposition activity of the **4R** sample when compared to the **5HT** sample is suggestive of another factor not examinable by XPS or XRD. Therefore, HAADF-STEM was performed on the samples to provide a greater insight into the particle size changes suggested by XRD and XPS. Comparison of fresh **5R** and **5HT** 2.6 wt. % Pd-Al_2O_3 samples

by electron microscopy are shown in Fig. 4. The fresh catalyst possesses Pd particles in the range of 1-5 nm (Fig. 4a). Large Pd particles (> 10 nm) of PdO are present after five reaction cycles (Fig. 4b), however, small particles persist. These large particles were not present in the fresh catalyst and are, therefore, consistent with analysis of the XRD and XPS results. That is PdO particles have sintered to form large nano-particles greater than 10 nm. Liu *et al*. showed that sintering is a common mechanism by which metal surface area and dispersion decreases [69,70]. In the 5HT sample, HAADF-STEM shows that there are a range of particle sizes visible with both large particles (> 5 nm) and small (< 2 nm) present. In general, the presence of the large nanoparticles indicates that during the heat treatments sintering occurred and despite the removal of Cl^- ions an increase in activity was not realised, due to the concomitant the loss of metal surface area. The increase in activity of the Fresh catalyst with multiple use is due to incremental removal of Cl^- ions, with a slight decrease in activity seen after the 4th cycle (**4R**) as the effect of the removal of Cl is negated by the formation of larger Pd nano-particles, as seen by HAADF-STEM in the **5R** sample. Representative particle size distributions could not be constructed due the presence of non-spherical agglomerates of nano-particles that would produce a statistically irrelevant distribution.

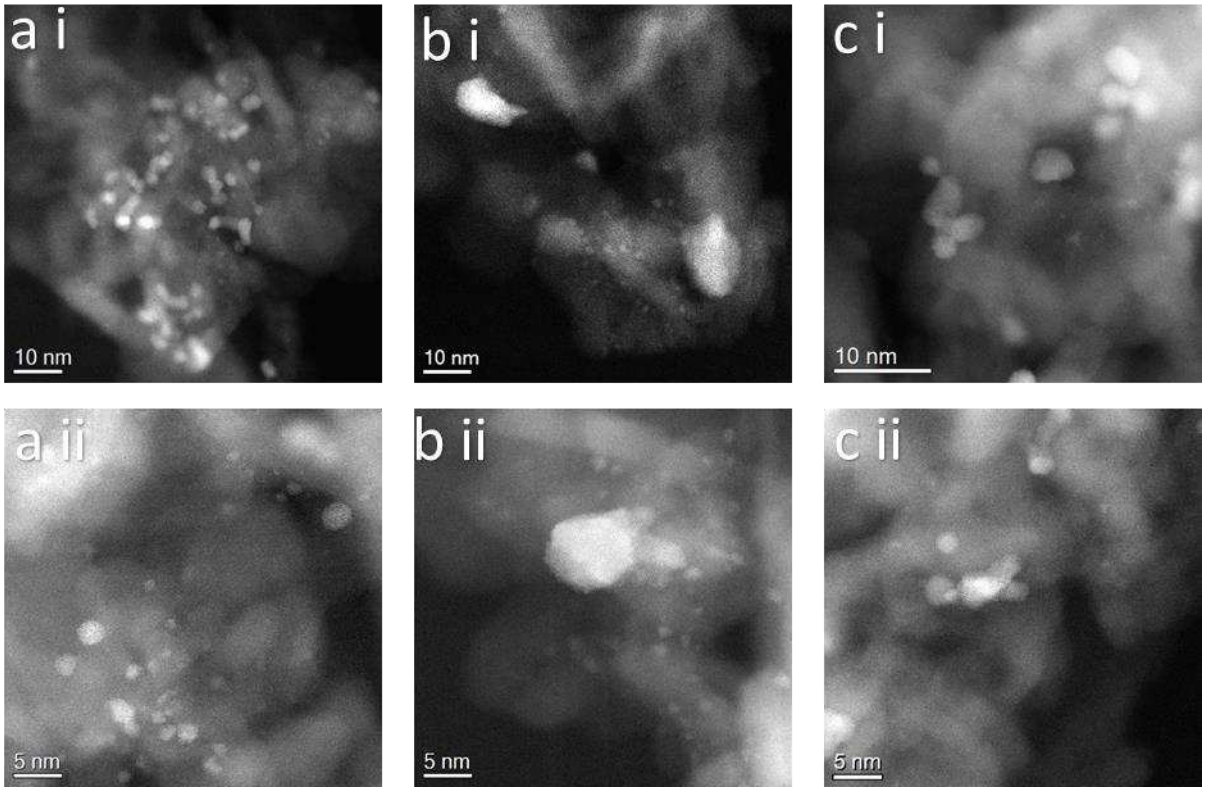

Fig. 4. HAADF-STEM images of 2.6 wt. % Pd-Al_2O_3 Fresh (a), 5R (b), and 5 HT (c).

These initial results suggest that alongside the presence of Cl^-, the size of the Pd particles strongly contribute to the rate of N_2O decomposition. To try to achieve similar levels of activity as the catalyst which has undergone four reaction cycles a preparatory method to control Pd particle sizes was explored. This would negate the need to carry out multiple catalyst test cycles. As Al_2O_3 is hygroscopic, it was hypothesised that the removal of surface water species and carbonates (the C 1s region of the XPS spectra showed peak at 289.7 eV, that is indicative of O-C=O, carbonate species) could enhance the dispersion of Pd, as these species may block the pore structure of the support [71,72]. Therefore, the alumina support was calcined under flowing air at 600 °C at 10 °C min^{-1} for 4 h before metal deposition (denoted as **SC**) and a 2.6 wt. % Pd-Al_2O_3 catalyst was then prepared by wet impregnation. Analysis of the calcined alumina supported the inference of water removal from the surface through calcination, as illustrated by solid state magic angle spinning (MAS) ^1H NMR (Fig. 5).

The properties of the untreated, as-received Al_2O_3 and calcined Al_2O_3 were investigated by NMR (Fig. 5**Error! Reference source not found.**). Both spectra contain a single broad peak that is associated to the protons of physisorbed water. The difference in broadness is related to the quantity of water absorbed on the surface of the support. The spectra suggest that there are more physisorbed water molecules present on the untreated sample compared to that of the calcined sample. Both spectra reveal a significant resonance at 4.6 ppm that corresponds to hydrogen bonded water on the Al_2O_3 surface. Spectra of the untreated sample has a shoulder present that is not present in the calcined sample, this shoulder at 1.2 ppm is due to the presence of non-hydrogen bonded physisorbed water [73,74]. In this spectra there is also a slight shoulder at 7 ppm; this resonance is due to Brønsted acid sites that are produced when water adsorbs onto a Lewis acidic site [75]. The absence of these two shoulder resonances indicates that water was removed during the calcination treatment.

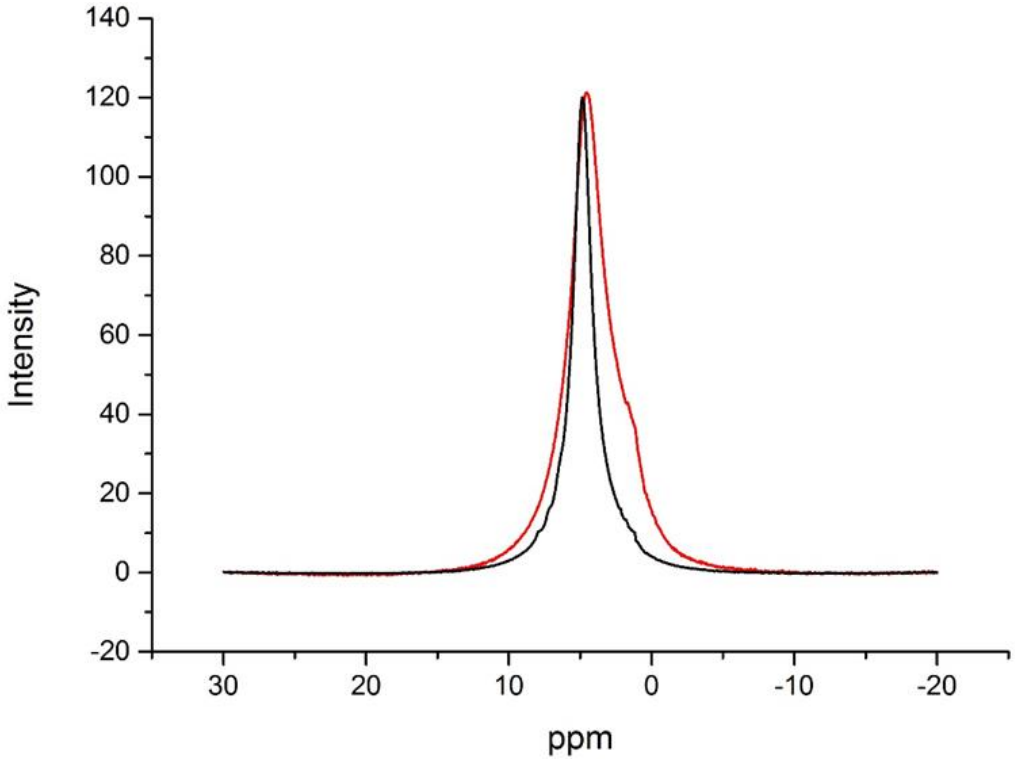

Fig. 5. Solid-state ^{1}H NMR spectrum of Al_2O_3 Fresh (red) and calcined (black)

Furthermore, calcination of the support led to a change in the point of zero charge (PZC) of the γ-Al_2O_3, from PZC = 8.43 for the untreated support, to 8.04 after calcination (see supplementary information Fig. S1 and Fig. S2). The measured pH of the $PdCl_2$ solution used to prepare the catalysts was 1.0, and the Pd solution was confirmed to comprise of $PdCl_3(H_2O)^-$ by Raman spectroscopy (see supplementary information Fig. S3). When the pH of the solution is lower than that of the PZC, the surface will be protonated and will strongly interact with anions [76,77] therefore the decrease in PZC of the calcined catalyst will mean the surface is less positively-charged during the catalyst preparation. This modification in surface charge may be beneficial for the dispersion of the Pd nanoparticles on the support, as is the case for the preparation of gold catalysts by deposition-precipitation.[78] Therefore the 2 wt. % Pd-Al_2O_3 **SC** would be expected to have a better dispersion than the palladium supported on the untreated support. An accurate Pd weight loading on both the fresh and **SC** Pd-Al_2O_3 catalysts was performed with ICP-OES, both catalysts had a 2.61 wt. % Pd loading.

HAADF-STEM shows that similar Pd nanostructures are present in the fresh and **SC** catalysts with nanoparticles and clusters present in both samples (Fig. 6). However, HAADF-STEM indicates that in the **SC** catalyst there are an increased quantity of small nanoparticles than in the fresh catalyst (Fig. 6b). The HAADF-STEM of the **SC** catalyst featured many nanoparticles less than 1 nm and some nanoparticles in the range of 3 – 8 nm. When compared to the **5R** catalyst which has undergone multiple reaction cycles there are significantly more smaller nanoparticles present in the **SC** catalyst

(Fig. 6b). For the **5R** sample (Fig. 4b) there are no nanoparticles that are sub 1 nm, whereas these are easily identifiable in the SC catalyst (Fig. 6b).

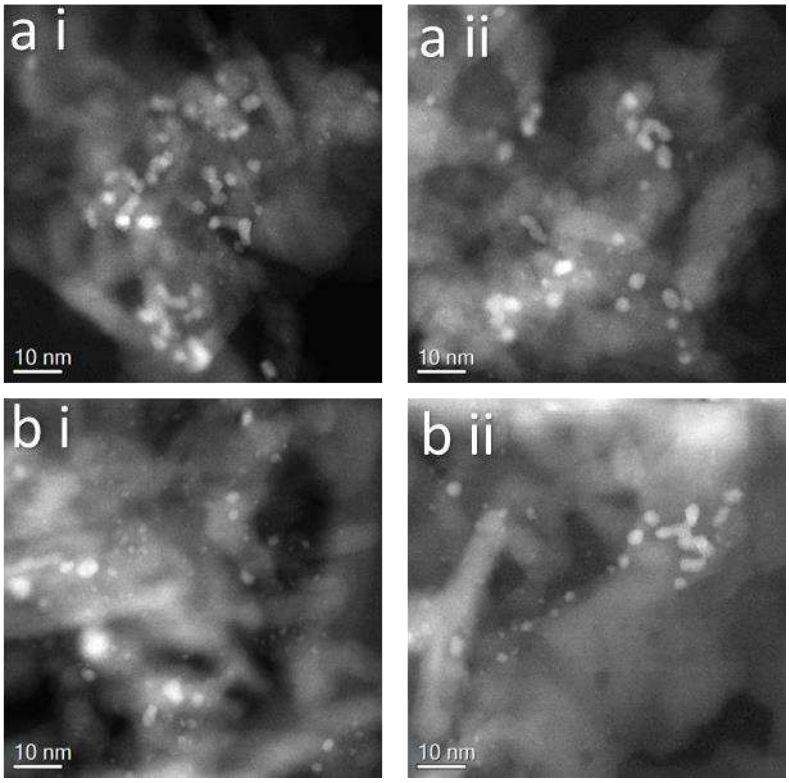

Fig. 6. HADDF-STEM images of 2.6 wt. % Pd-Al_2O_3 Fresh (a) and Support calcined (**SC**) (b)

The SC catalyst was evaluated for N_2O decomposition and compared to the fresh and **5R** catalysts (Fig. 7). The T_{50} obtained over the **SC** catalyst was found to be 561 °C and compared to the values of 577 and 540 °C over the fresh and **5R** catalysts. Therefore, the support pre-treatment step has increased the N_2O decomposition rate to 15.9 mol_{N2O} h^{-1} kg_{cat}^{-1} at 550 °C and is indicative of the formation of a higher density of active Pd nano-particles. Performing, a comparable reaction cycle with the **SC** catalyst resulted in a modest increase of the decomposition rate to 18.8 mol_{N2O} h^{-1} kg_{cat}^{-1} at 550 °C and a decrease of the T_{50} to 556 °C over the fifth use catalyst (**SC 5R**). We consider the modest improvement in the decomposition rate suggests that the PdCl population has decreased as with the **5R** sample.

It has been shown previously that adding a reductant (such as propane [45–49]) to the gas feed lowers the temperature required for 100 % conversion. This is due to the rate limiting step of N_2O decomposition being the desorption and recombination of oxygen to form O_2 [38–44]. Propane acts as reductant that can facilitate the abstraction of oxygen from the oxidised active site, significantly increasing the observed rate of N_2O decomposition at lower temperatures [27,28]. In this case the

presence of propane lowers the temperature required by almost 200 °C. Reactions were carried out with the addition of propane in the gas feed (1 %). The dramatic increase in decomposition activity is observed with all catalysts but is most noticeable with the **SC** catalyst, as with N_2O only, 95 % conversion is achieved at 600 °C, in the presence of propane 95 % conversion is achieved at 350 °C.

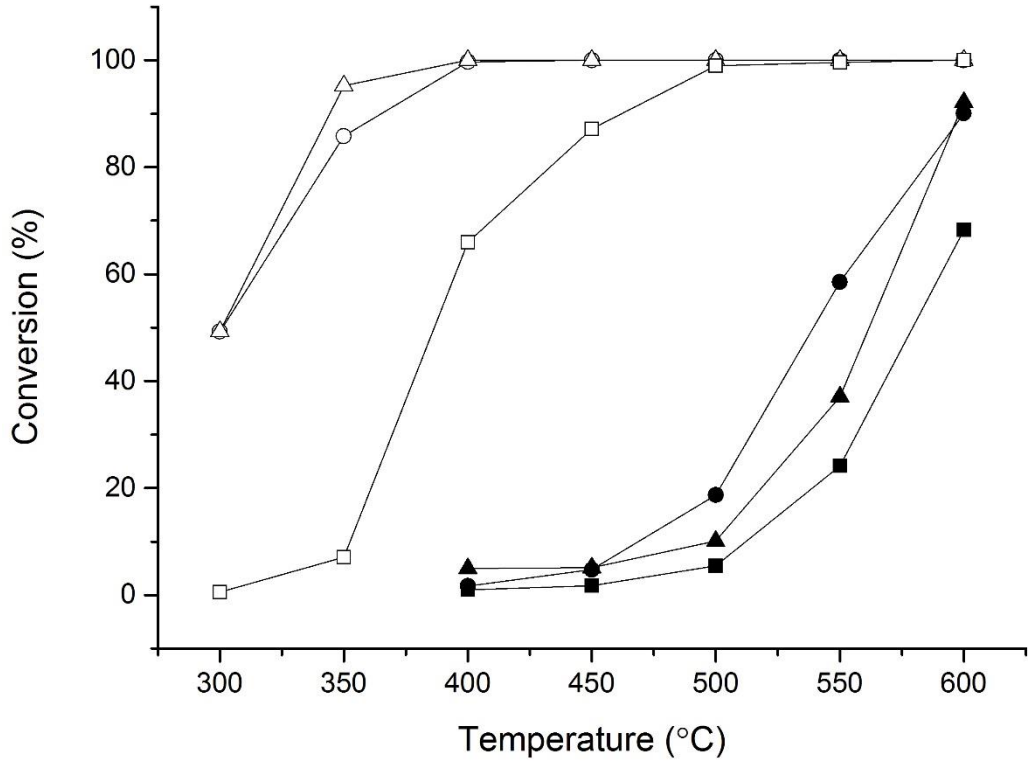

Fig. 7. The effect on N_2O conversion of heat treatments on 2.6 wt. % Pd-Al_2O_3. Reaction Conditions: total flow 100 mL min^{-1}, GHSV: 76690 h^{-1}, 300 - 600 °C, Closed symbols: 1 % N_2O/He, Open symbols: 1 % N_2O/1 % C_3H_8/He. Legend: ■ - 2.6 wt. % Pd-Al_2O_3 Fresh, ● - 2.6 wt. % Pd-Al_2O_3 5R, ▲- 2.6 wt. % Pd-Al_2O_3 SC.

The superior dispersion Pd on the **SC** catalyst, as evidenced by HAADF-STEM implies that the anchoring of Pd is stronger on the calcined support. To examine directly the stability of the Pd species on the surface of the Al_2O_3, *in situ* XRD was performed. The *in situ* XRD profiles of 2.6 wt. % Pd-Al_2O_3 and **SC** catalysts are illustrated in Fig. 8a and b, respectively. The samples were heated in 1 % N_2O/N_2 and cooled in N_2 at 50 °C intervals. The *in situ* XRD patterns of 2.6 wt. % Pd-Al_2O_3 shows that small PdO reflections were present at 500 °C, with the intensity of the PdO reflections not increasing past 550 °C, with Pd^0 reflections forming at the same temperatures. In the **SC** catalyst PdO and Pd reflections were not visible until at least 600 °C. The difference in temperature required to observe reflections corresponding to nanoparticles of PdO and Pd indicates that the Pd nanoparticles are more strongly anchored to the calcined Al_2O_3 than the untreated support. The effect of the reaction time-on-line was investigated, (Fig. S4), and the fresh catalyst sharply loses activity over the first 3 h, before following

a downward trend over the next 15 h. This catalyst is not stable during long term reactions. However, the **SC** catalyst shows promise, initially there is a decrease in activity in the first hour but the activity then improves, and the catalyst is stable over an 18 h period with the conversion of N_2O remaining constant. These observation are in agreement with the *in situ* XRD data.

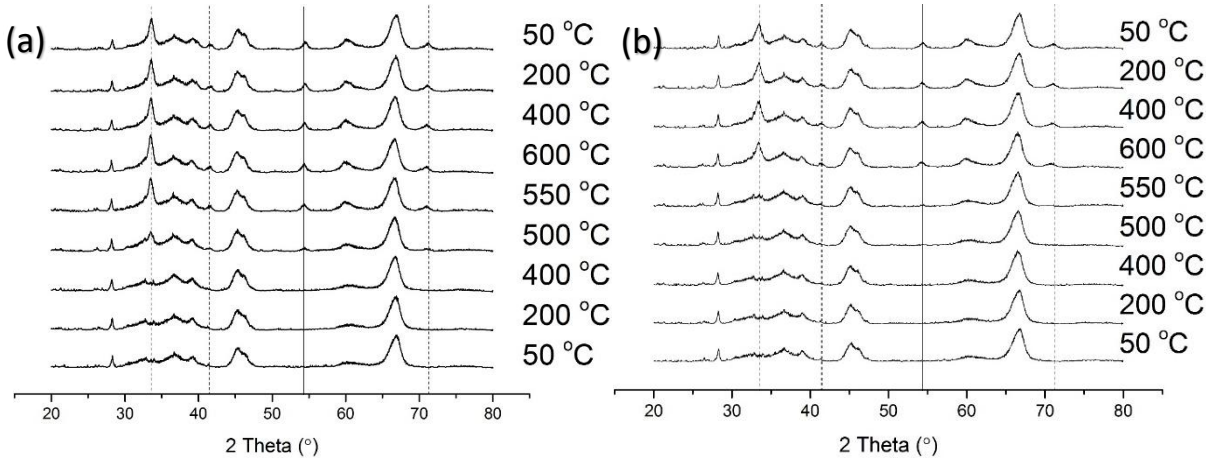

Fig. 8. *In situ* XRD patterns taken at regular temperature intervals for (a) 2.6 wt. % Pd-Al_2O_3 Fresh and (b) 2.6 wt. % Pd-Al_2O_3 **SC** heated in 1 % N_2O/N_2 and then cooled in N_2. Solid Line; Pd, Dashed line; PdO.

The average particle size of the Pd present on the surface was further investigated with CO chemisorption of the fresh and **SC** catalysts. It is assumed that all Pd particles are hemispherical and that one CO molecule will bind to one Pd atom, STEM has shown this is not the case but this will give an average particle size and metal surface area. Metal nanoparticle dispersion increased modestly from 24.7 % to 27.5 % with the fresh to the **SC** catalyst (Table 3). The average particle size of Pd particles in the **SC** catalyst decreased when compared to the fresh catalyst. This decrease in average particle size indicated that the nanoparticles found on the **SC** catalyst are smaller and further support the inference that smaller particles are more active than larger particles for N_2O decomposition. This is due to the smaller particles having a larger surface area per gram of metal and this small change in particle size facilitates an increased decomposition reaction rate through the increased surface area available.

Table 3. Dispersion and metal surface area as calculated by CO Chemisorption on 2.6 wt. % Pd-Al_2O_3 fresh and SC.

Catalyst	Metal Surface Area ($m^2\ g^{-1}$)	Avg. particle size (nm)	Dispersion (%)
2.6 wt. % Pd-Al_2O_3 Fresh	2.9	1.51	24.7
2.6 wt. % Pd-Al_2O_3 **SC**	3.2	1.36	27.5

The catalytic activity for N_2O decomposition when propane is present with the fresh and **SC** catalysts is markedly different (Fig. 7). To investigate the effect of particle size, the catalysts were re-prepared using a modified impregnation (**MI**) technique which has been shown previously to produce catalysts with a very narrow particle size distribution [58]. Palladium was deposited with the MI technique on a calcined alumina and an as-received alumina and examined by XPS, XRD, CO chemisorption and HAADF-STEM. The Pd loading of the MI prepared catalysts was analysed by ICP-OES and was found to be lower (2.1 wt.%) than the traditionally prepared impregnation catalysts (2.6 wt. %). The materials were examined by CO chemisorption (Table 4) and this revealed that the average Pd particle size, 1.25 and 1.28 nm was smaller than the analogue impregnation catalysts displayed in Table 3. However, the metal surface area was found to be lower and can be assigned to the lower Pd loading of the **MI** catalysts. When comparing the XRD patterns of 2.1 wt. % Pd-Al_2O_3 **MI** catalysts, it is clear that there are no Pd or PdO reflections (see supplementary information Fig. S5). This indicates that the Pd species are smaller than the detection limit of XRD, which is consistent with the CO chemisorption data.

Table 4. Dispersion and metal surface area as calculated by CO Chemisorption on 2.1 wt. % Pd-Al_2O_3 fresh and **SC** prepared by modified impregnation.

Catalyst	**Metal Surface Area (m^2 g^{-1})**	**Avg. particle size (nm)**	**Dispersion (%)**
2.1 wt.% Pd-Al_2O_3 Fresh **MI**	2.8	1.25	29.8
2.1 wt.% Pd-Al_2O_3 **SC MI**	2.7	1.28	29.3

The modified impregnation technique requires an excess of HCl to be added during the preparation. This facilitates the deposition of Pd and the subsequently observed metal particle control, through altering the support PZC and inducing an increased interaction between the Pd precursor and the support. Characterisation by XPS shows a high ratio of PdO to PdCl in the modified impregnation catalysts. For both the un-calcined supported catalyst (2.1 wt. % Pd-Al_2O_3 Fresh **MI**) and the calcined supported catalyst (2.1 wt. % Pd-Al_2O_3 **SC MI**), there is an elevated population of Pd-Cl species compared to PdO species, despite undergoing calcination (Fig. 9**Error! Reference source not found.**

and Table 5). In contrast, when comparing the ratio of PdO to PdCl species for the 2.6 wt. % Pd-Al_2O_3 **SC** catalyst was found to have more PdO present than PdCl.

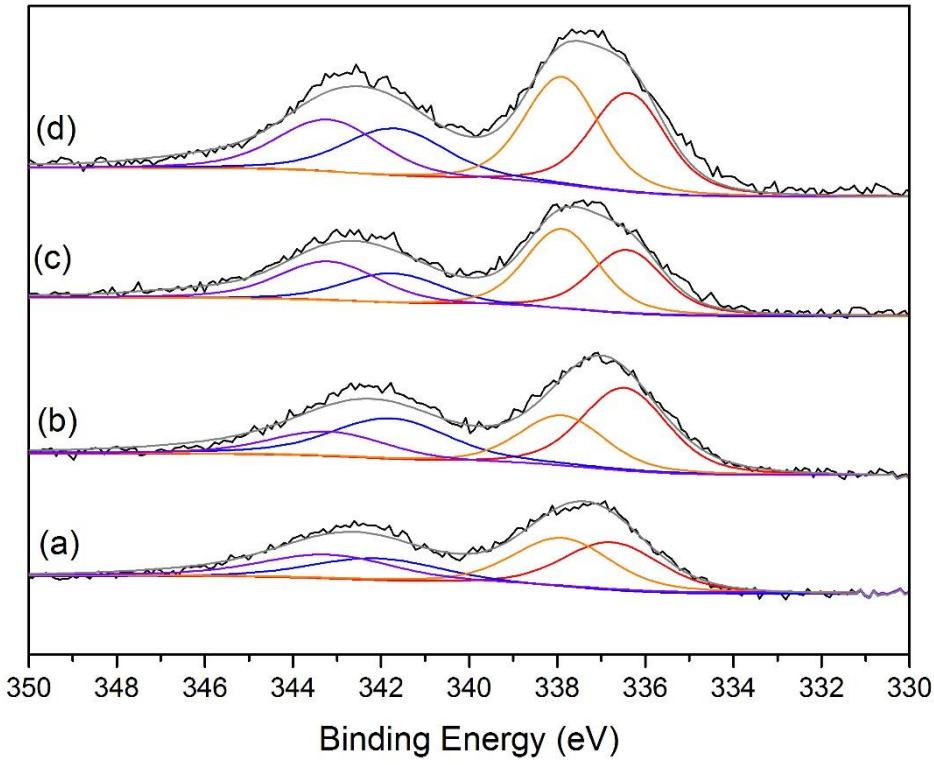

Fig. 9. XPS spectra for fresh or SC Pd-Al_2O_3 catalysts prepared by impregnation (2.6 wt. % Pd) or Modified Impregnation (2.1 wt. % Pd). Legend: (a) Fresh, (b) **SC**, (c) **MI**, (d) **MI SC**. Each spectra is fitted with two peaks corresponding to PdO and PdCl species. Legend: Red and Blue – PdO, Orange and Purple – PdCl.

Table 5. Surface composition of Pd- Al_2O_3 catalysts as reported by XPS analysis

Catalyst	**Pd 3d (at.%)**	**% of PdO (337 eV) (%)**	**% of PdCl (339 eV) (%)**
2.6 wt. % Pd-Al_2O_3 **SC**	0.48	62.3	37.7
2.1 wt. % Pd-Al_2O_3 Fresh **MI**	0.39	43.5	56.5
2.1 wt. % Pd-Al_2O_3 SC **MI**	0.42	47.6	52.3

The 2.1 wt.% Pd/Al_2O_3 **MI** and 2.1 wt.% Pd/Al_2O_3 **SC MI** catalysts were tested for N_2O decomposition with and without propane present and compared to the equivalent impregnation catalysts (Fig. 10.a and b). When only N_2O is present in the gas feed there is still minor difference in activity, with the **SC MI** catalyst modestly outperforming, that of the fresh **MI** catalyst (Fig. 10.a). The **MI** catalysts outperform the corresponding impregnation catalysts, and further support the supposition that the N_2O decomposition reaction is sensitive to the active surface composition and structure. This reactivity can be attributed to the increased dispersion of smaller and more active metal particles available for

391 N_2O decomposition to occur, based on the results from CO Chemisorption (Table 4). However, the
392 increased Cl^- on the surface of the **MI** catalysts restricts the activity to only the minor improvement
393 observed. The T_{50} obtained over the **MI** catalyst was found to be 576 °C and compared to the values
394 of 547 °C over the **MI SC** catalyst. Therefore, the support pre-treatment step has increased the N_2O
395 decomposition rate from 16.3 mol_{N2O} h^{-1} kg_{cat}^{-1} to 21.9 mol_{N2O} h^{-1} kg_{cat}^{-1} at 550 °C.

396 When propane was added to the reaction mixture the effect of calcining the support prior to Pd
397 deposition was negated (Fig. 10b). The activity of the **MI** catalysts was lower, at *ca*. 78 % N_2O
398 conversion compared to that of the **SC** catalyst, but higher than that of the fresh supported Al_2O_3
399 catalyst at 350 °C, compared to 96 % for **SC** and 7 % for the fresh catalyst (Fig. 10a). As the activity of
400 both **MI** catalysts was comparable the decomposition rate was *ca*. 30 mol_{N2O} h^{-1} kg_{cat}^{-1} at 350 °C with
401 propane present. It is possible that residual chlorine species may inhibit the reaction as observed with
402 the catalysts that underwent increasing reaction cycles. However, it is clear that the influence of
403 calcining the support prior to metal impregnation is negated with the **MI** catalysts for this reaction
404 with propane.

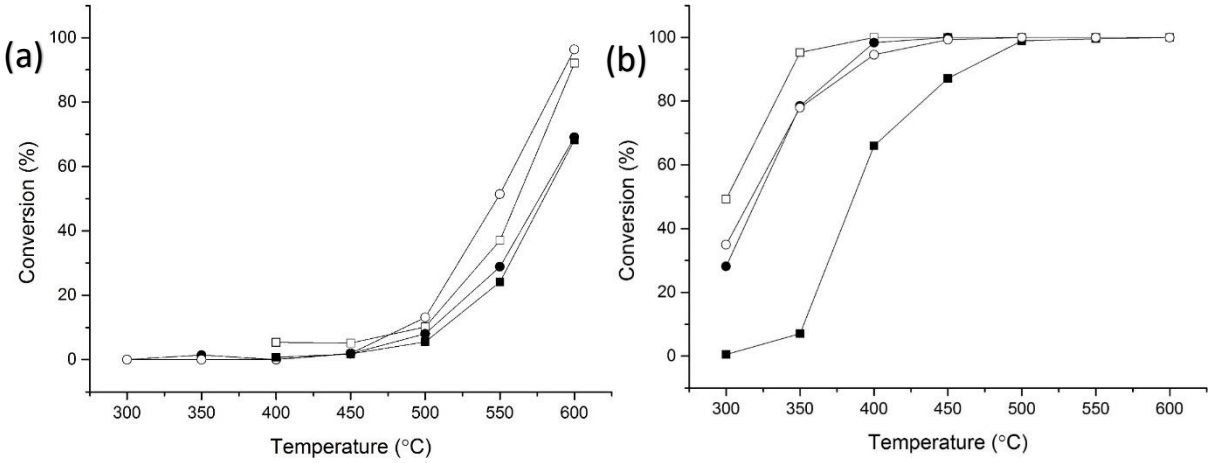

405

406 Fig. 10. The effect on N_2O conversion of catalyst preparation over Pd-Al_2O_3 Fresh (filled symbols) and
407 **SC** catalysts (open symbols): ■ - 2.6 wt.% Pd Fresh, □ - 2.6 wt.% Pd SC, ● - 2.1 wt.% Pd **MI**, ○ - 2.1
408 wt.% Pd **SC MI**. Reaction conditions; (a), 1 % N_2O/He, total flow 100 ml min^{-1}, GHSV: 75900 h^{-1}, (b), 1 %
409 N_2O/1 % C_3H_8/He, total flow 100 ml min^{-1}, GHSV: 75900 h^{-1}.

410

411 HAADF-STEM images of the fresh **MI** catalyst (Fig. 11a) and the post-reaction **MI** catalyst (Fig. 11b)
412 show small, uniform particles that sinter after multiple uses. The particles that are present on the
413 fresh **MI** catalyst are sub 2 nm, with only a few particles larger than 2 nm. After one reaction cycle,
414 some of the particles present were measured to be *ca*. 5 nm, indicating that Pd sintering has taken
415 place. We consider that although the modified impregnation technique does provide increased
416 control over the metal nano-particle size it does not control the metal-support interaction. In theory,

the modified impregnation solution is more acidic due to the presence of HCl so the surface of the support is more positively charged. The consequence of this should be a stronger interaction between the precursor and the support, resulting in an increased metal dispersion compared to a conventional impregnation technique. However, as the support is not calcined it can be hypothesised that the interaction between the smaller particles produced by MI and the support may not be sufficiently strong due to the presence of water and can diminish the strength at which the Pd can anchor to the support and consequently lead to sintering.

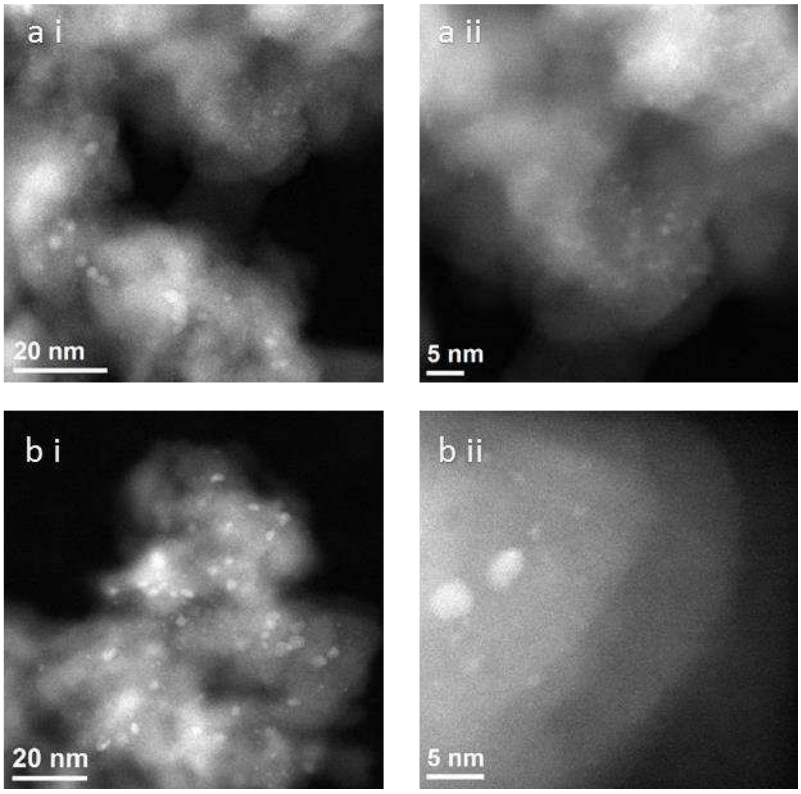

Fig. 11. HAADF-STEM images of 2.1 wt. % Pd-Al_2O_3 **MI** (a) **MI** fresh, (b) catalyst following one reaction cycle (**MI 1R)**.

Table 6. Comparison of the key catalysts in this manuscript with literature examples.

Catalyst	**T_{50}[a] (°C)**	**Conversion at 550 °C (%)**	**Decomposition Rate at 550 °C (mol_{N2O} h^{-1} kg_{cat}^{-1})**	**T_{100}[b] in the presence of propane (°C)**	**Ref**
Blank	-	0	0	-	This work
2.6 wt. % Pd-Al_2O_3 **Fresh**	577	24	10.3	550	This work
2.6 wt. % Pd-Al_2O_3 **4R**	527	67	28.7	-	This work
2.6 wt. % Pd-Al_2O_3 **5R**	540	57	24.4	400	This work

2.6 wt. % Pd-Al_2O_3 **5HT**	584	22	9.4	450	This work
2.6 wt. % Pd-Al_2O_3 **SC**	562	37	15.9	400	This work
2.1 wt. % Pd-Al_2O_3 **MI**	576	29	12.42	450	This work
2.1 wt. % Pd-Al_2O_3 **MI SC**	548	52	22.3	450	This work
2 wt. % Pd-Al_2O_3	350	100	2.6	400	Pekridis [27]
0.5 wt. % Pd-Al_2O_3	536	52	20.9	-	Tzitzios [56]
1 wt. % Pd-Al_2O_3	525	59	23.7	-	Pachatouridou [57]

[a] the temperature at 50 % N_2O conversion; [b] the temperature at 100 % N_2O conversion in the presence of propane.

428

429 The reactivity data (Table 6) highlights the structural sensitivity of the active site and how important
430 the relationship between Pd dispersion and presence of PdCl is. The increase in Pd dispersion resulted
431 in an increase in activity as seen when the support is calcined before catalyst preparation. However,
432 removal of Cl^- from the catalyst surface as with the catalysts that have undergone four or five reaction
433 cycles can lead to an improvement in activity despite the onset of Pd sintering and reduced Pd
434 dispersion. Further activity gains can be observed through careful control of the Pd dispersion, through
435 the MI technique despite a high density of PdCl. Therefore, the balance between a high Pd dispersion
436 and the presence of PdCl appears to favour the former. For comparison the previous literature data
437 are included in Table 6, and these demonstrate that the catalyst preparation conditions are key to
438 designing an active catalyst.

439

4 Conclusions

The effect of heat treatment conditions on a 2.6 wt. % Pd-Al_2O_3 catalysts have been investigated for the catalytic decomposition of N_2O into N_2 and O_2 in the absence and presence of a reducing agent (C_3H_8). It was found that the use of several reaction cycles increases the conversion of N_2O from 24 % to 57 % at 600 °C. These multiple use catalysts also show improved stability on-stream. It has also been demonstrated that by calcining the support before catalyst preparation, similar conversions as the multiple use catalyst can be achieved in the first cycle of the **SC** catalyst. This procedure enables the high activity to be achieved on the initial use rather than on the 5th cycle (**5R**). We consider that this is due to the removal of water species lowering the PZC of the support, which suggests a reduced interaction between the Pd ion and the support surface, leading to the formation of smaller nanoparticles. When a reductant is present the temperature at which *ca.* 100 % conversion is observed is decrease from 550 °C to 350 °C. The presence of the reductant enhances the decomposition of N_2O to N_2, however a limited amount of O_2 is measured, suggesting that the reductant was acting as a scavenger of oxygen to form cracked, oxidation products and water. When the support was calcined before catalyst preparation, the resultant catalyst was formed of small Pd nanoparticles. Reaction data indicate that small nanoparticles are the more active species, as when the particle size is controlled by using a modified impregnation preparation method the activity of both catalysts is the same, therefore further supporting the hypothesis that the particle size and subsequently the metal dispersion control the activity of a Pd-Al_2O_3 catalysts for N_2O decomposition.

5 Acknowledgements

ERC Funding 'After the GoldRush' code, ERC-AtG-291319. We would like to thank Exeter Analytical for the ICP-OES data, Durham University for Solid state NMR, Oakridge National Laboratory for HAADF-STEM images and the Catalysis Hub for use of the ChemBET pulsar machine.

6 References

[1] J. Pérez-Ramírez, F. Kapteijn, K. Schöffel, J.A. Moulijn, Formation and control of N2O in nitric acid production: Where do we stand today?, Appl. Catal. B Environ. 44 (2003) 117–151. doi:10.1016/S0926-3373(03)00026-2.

[2] J. Weimann, Toxicity of nitrous oxide., Best Pract. Res. Clin. Anaesthesiol. 17 (2003) 47–61. http://www.ncbi.nlm.nih.gov/pubmed/12751548.

[3] P. Grace, L. Barton, http://theconversation.com/meet-n2o-the-greenhouse-gas-300-times-worse-than-co2-35204, Http://Theconversation.Com/Meet-N2o-the-Greenhouse-Gas-300-Times-Worse-than-Co2-35204. (n.d.) 2015-10–29.

[4] Intergovernmental Panel on Climate Change, Climate Change 2007 Synthesis Report, 2008. doi:10.1256/004316502320517344.

[5] L. Li, J. Xu, J. Hu, J. Han, Reducing nitrous oxide emissions to mitigate climate change and protect the ozone layer, Environ. Sci. Technol. 48 (2014) 5290–5297. doi:10.1021/es404728s.

[6] Intergovernmental Panel on Climate Change, Climate Change 2013: The Physical Science Basis. Contribution of Working Group I to the Fifth Assessment Report of the Intergovernmental Panel on Climate Change, 2013. doi:10.1017/CBO9781107415324.

[7] M. Jabłońska, R. Palkovits, It is no laughing matter: Nitrous oxide formation in diesel engines and advances in its abatement over rhodium-based catalysts, Catal. Sci. Technol. 6 (2016) 7671–7687. doi:10.1039/c6cy01126h.

[8] UNEP, Drawing Down Nitrous Oxide To Protect Climate and the Ozone Layer, 2013. doi:10.13140/2.1.4720.8646.

[9] S.S. Maroufi, M.J. Gharavi, M. Behnam, A. Samadikuchaksaraei, Nitrous oxide levels in operating and recovery rooms of Iranian hospitals, Iran. J. Public Health. 40 (2011) 75–79.

[10] F. Kapteijn, J. Rodriguez-Mirasol, J.A. Moulijn, Heterogeneous catalytic decomposition of nitrous oxide, Appl. Catal. B Environ. 9 (1996) 25–64. doi:10.1016/0926-3373(96)90072-7.

[11] S. Kumar, Y. Teraoka, A.G. Joshi, S. Rayalu, N. Labhsetwar, Ag promoted La0.8Ba0.2MnO3 type perovskite catalyst for N2O decomposition in the presence of O2, NO and H2O, J. Mol. Catal. A Chem. 348 (2011) 42–54. doi:10.1016/j.molcata.2011.07.017.

[12] S. Kumar, A. Vinu, J. Subrt, S. Bakardjieva, S. Rayalu, Y. Teraoka, N. Labhsetwar, Catalytic N2O decomposition on Pr0.8Ba 0.2MnO3 type perovskite catalyst for industrial emission control, Catal. Today. 198 (2012) 125–132. doi:10.1016/j.cattod.2012.06.015.

[13] J.P. Dacquin, C. Lancelot, C. Dujardin, P. Da Costa, G. Djega-Mariadassou, P. Beaunier, S. Kaliaguine, S. Vaudreuil, S. Royer, P. Granger, Influence of preparation methods of LaCoO3on the catalytic performances in the decomposition of N2O, Appl. Catal. B Environ. 91 (2009) 596–604. doi:10.1016/j.apcatb.2009.06.032.

[14] K.K. Kartha, M.R. Pai, A.M. Banerjee, R. V. Pai, S.S. Meena, S.R. Bharadwaj, Modified surface and bulk properties of Fe-substituted lanthanum titanates enhances catalytic activity for CO + N2O reaction, J. Mol. Catal. A Chem. 335 (2011) 158–168. doi:10.1016/j.molcata.2010.11.028.

[15] N. Russo, D. Mescia, D. Fino, G. Saracco, V. Specchia, N2O decomposition over perovskite catalysts, Ind. Eng. Chem. Res. 46 (2007) 4226–4231. doi:10.1021/ie0612008.

[16] M. Zabilskiy, B. Erjavec, P. Djinović, A. Pintar, Ordered mesoporous CuO-CeO2 mixed oxides as

504 an effective catalyst for N2O decomposition, Chem. Eng. J. 254 (2014) 153–162.
505 doi:10.1016/j.cej.2014.05.127.

506 [17] H. Zhou, P. Hu, Z. Huang, F. Qin, W. Shen, H. Xu, Preparation of NiCe mixed oxides for catalytic
507 decomposition of N2O, Ind. Eng. Chem. Res. 52 (2013) 4504–4509. doi:10.1021/ie400242p.

508 [18] H. Zhou, Z. Huang, C. Sun, F. Qin, D. Xiong, W. Shen, H. Xu, Catalytic decomposition of N2O over
509 CuxCe1-xOymixed oxides, Appl. Catal. B Environ. 125 (2012) 492–498.
510 doi:10.1016/j.apcatb.2012.06.021.

511 [19] B.M. Abu-Zied, S.A. Soliman, S.E. Abdellah, Enhanced direct N2O decomposition over CuxCo1-
512 xCo2O4(0.0≤x≤1.0) spinel-oxide catalysts, J. Ind. Eng. Chem. 21 (2015) 814–821.
513 doi:10.1016/j.jiec.2014.04.017.

514 [20] P. Stelmachowski, G. Maniak, J. Kaczmarczyk, F. Zasada, W. Piskorz, A. Kotarba, Z. Sojka, Mg
515 and Al substituted cobalt spinels as catalysts for low temperature deN2O-Evidence for
516 octahedral cobalt active sites, Appl. Catal. B Environ. 146 (2014) 105–111.
517 doi:10.1016/j.apcatb.2013.05.027.

518 [21] R. Amrousse, A. Tsutsumi, A. Bachar, D. Lahcene, N2O catalytic decomposition over nano-sized
519 particles of Co-substituted Fe3O4 substrates, Appl. Catal. A Gen. 450 (2013) 253–260.
520 doi:10.1016/j.apcata.2012.10.036.

521 [22] S. Parres-Esclapez, M.J. Illan-Gomez, C.S.M. de Lecea, A. Bueno-Lopez, On the importance of
522 the catalyst redox properties in the N2O decomposition over alumina and ceria supported Rh,
523 Pd and Pt, Appl. Catal. B Environ. 96 (2010) 370–378. doi:10.1016/j.apcatb.2010.02.034.

524 [23] K. Yuzaki, T. Yarimizu, S. Ito, K. Kunimori, Catalytic decomposition of N2O over supported
525 rhodium catalysts: high activities of Rh/USY and Rh/Al2O3 and the effect of Rh precursors,
526 Catal. Letters. 47 (1997) 173–175.
527 http://link.springer.com/article/10.1023/A:1019017407609.

528 [24] F. Kapteijn, G. Mul, G. Marbán, J. Rodriguez-Mirasol, J.A. Moulijn, Decomposition of nitrous
529 oxide over ZSM-5 catalysts, in: 11th Int. Congr. Catal. - 40th Anniv. Vol. 101, 1996: pp. 641–
530 650. doi:10.1016/S0167-2991(96)80275-8.

531 [25] C. Kordulis, H. Latsios, A. Lycourghiotis, P. Pomonis, Kinetics of N2o Decomposition on Fe-3+
532 Supported on Pure and Li-Modified Al2o3, Int. J. Chem. Tech. Res. 88 (2015) 201–205.
533 doi:10.1016/j.physe.2016.11.016.

534 [26] Y. Li, J.N. Armor, Catalytic decomposition of nitrous oxide on metal exchanged zeolites, Applied
535 Catal. B, Environ. 1 (1992) 1–9. doi:10.1016/0926-3373(92)80019-V.

536 [27] G. Pekridis, C. Athanasiou, M. Konsolakis, I. V. Yentekakis, G.E. Marnellos, N2O abatement over
537 gamma-Al2O3 supported catalysts: Effect of reducing agent and active phase nature, Top.
538 Catal. 52 (2009) 1880–1887. doi:10.1007/s11244-009-9346-6.

539 [28] S.C. Christoforou, E.A. Efthimiadis, I.A. Vasalos, Catalytic conversion of N 2 O to N 2 over metal-
540 based catalysts in the presence of hydrocarbons and oxygen, Catal. Letters. 79 (2002) 137–147.

541 [29] M. Machida, T. Watanabe, S. Ikeda, T. Kijima, A dual-bed lean deNOx catalyst system consisting
542 of NO-H 2-O2 reaction and subsequent N2O decomposition, Catal. Commun. 3 (2002) 233–
543 238. doi:10.1016/S1566-7367(02)00091-2.

544 [30] Y. Tateishi, T. Tsuneyuki, H. Furukawa, S. Kagawa, I. Moriguchi, Y. Kanmura, Y. Teraoka,
545 Investigation on catalysts for the direct decomposition of nitrous oxide for waste anesthetic
546 gas purification, Catal. Today. 139 (2008) 59–63. doi:10.1016/j.cattod.2008.08.008.

[31] K. Doi, Y.Y. Wu, R. Takeda, A. Matsunami, N. Arai, T. Tagawa, S. Goto, Catalytic decomposition of N2O in medical operating rooms over Rh/Al2O3, Pd/Al2O3, and Pt/Al2O3, Appl. Catal. B Environ. 35 (2001) 43–51. doi:10.1016/S0926-3373(01)00231-4.

[32] K. Zorn, S. Giorgio, E. Halwax, C.R. Henry, H. Gronbeck, G. Rupprechter, CO Oxidation on Technological Pd - Al 2 O 3 Catalysts : Oxidation State and Activity, J. Phys. Chem. C. 115 (2011) 1103–1111. doi:10.1021/jp106235x.

[33] T. Maillet, C. Solleau, J. Barbier, D. Duprez, Oxidation of carbon monoxide, propene, propane and methane over a Pd/Al2O3 catalyst. Effect of the chemical state of Pd, Appl. Catal. B Environ. 14 (1997) 85–95. doi:10.1016/S0926-3373(97)00014-3.

[34] A.S. Ivanova, E.M. Slavinskaya, R. V. Gulyaev, V.I. Zaikovskii, O.A. Stonkus, I.G. Danilova, L.M. Plyasova, I.A. Polukhina, A.I. Boronin, Metal-support interactions in Pt/Al2O3and Pd/Al2O3catalysts for CO oxidation, Appl. Catal. B Environ. 97 (2010) 57–71. doi:10.1016/j.apcatb.2010.03.024.

[35] D. Roth, P. Gélin, A. Kaddouri, E. Garbowski, M. Primet, E. Tena, Oxidation behaviour and catalytic properties of Pd/Al2O3catalysts in the total oxidation of methane, Catal. Today. 112 (2006) 134–138. doi:10.1016/j.cattod.2005.11.048.

[36] D. Gao, C. Zhang, S. Wang, Z. Yuan, S. Wang, Catalytic activity of Pd/Al2O3toward the combustion of methane, Catal. Commun. 9 (2008) 2583–2587. doi:10.1016/j.catcom.2008.07.014.

[37] J. Lu, B. Fu, M.C. Kung, G. Xiao, J.W. Elam, H.H. Kung, P.C. Stair, Coking- and Sintering-Resistant Palladium Catalysts Achieved Through Atomic Layer Deposition, Science. 335 (2012) 1205–1208. doi:10.1126/science.1212906.

[38] H. Guesmi, D. Berthomieu, L. Kiwi-Minsker, Nitrous Oxide Decomposition on the Binuclear [Fe II (μ-O)(μ-OH)Fe II] Center in Fe-ZSM-5 Zeolite, J. Phys. Chem. C. 112 (2008) 20319–20328. doi:10.1021/jp808044r.

[39] C. Sang, B.H. Kim, C.R.F. Lund, Effect of NO upon N $_2$ O Decomposition over Fe/ZSM-5 with Low Iron Loading †, J. Phys. Chem. B. 109 (2005) 2295–2301. doi:10.1021/jp048884m.

[40] N. Hansen, A. Heyden, A.T. Bell, F.J. Keil, A Reaction Mechanism for the Nitrous Oxide Decomposition on Binuclear Oxygen Bridged Iron Sites in {Fe-ZSM-5}, J. Phys. Chem. C. 111 (2007) 2092–2101. doi:10.1021/jp065574q.

[41] D.A. Bulushev, L. Kiwi-minsker, A. Renken, Dynamics of N 2 O decomposition over Fe / ZSM-5 catalysts : effects of, Ind. Eng. Chem. Res. 211 (2004) 2004.

[42] K. Sun, H. Xia, E. Hensen, R. van Santen, C. Li, Chemistry of N2O Decomposition on active sites with different nature: Effect of high temperature treatment of Fe/ZSM-5, J. Catal. 238 (2006) 186–195. doi:10.1016/j.jcat.2005.12.013.

[43] G.D. Pirngruber, The surface chemistry of N2O decomposition on iron containing zeolites (I), J. Catal. 219 (2003) 456–463. doi:10.1016/S0021-9517(03)00220-3.

[44] B. R.Wood, J.A. Reimer, A.T. Bell, Studies of N2O Adsorption and Decomposition on Fe–ZSM-5, J. Catal. 209 (2002) 151–158. doi:10.1006/jcat.2002.3610.

[45] H. Ohtsuka, T. Tabata, O. Okada, L.M.F. Sabatino, G. Bellussi, A study on selective reduction of NOx by propane on Co-Beta, Catal. Letters. 44 (1997) 265–270.

[46] H. Ohtsuka, T. Tabata, O. Okada, L.M.. Sabatino, G. Bellussi, A study on the roles of cobalt species in NOx reduction by propane on Co-Beta, Catal. Today. 42 (1998) 45–50.

590 doi:10.1016/S0920-5861(98)00075-3.

591 [47] R.W. Van Den Brink, S. Booneveld, M.J.F.M. Verhaak, F.A. De Bruijn, Selective catalytic
592 reduction of N2O and NOx in a single reactor in the nitric acid industry, Catal. Today. 75 (2002)
593 227–232. doi:10.1016/S0920-5861(02)00073-1.

594 [48] G. Centi, F. Vazzana, Selective Catalytic Reduction of N2O in Industrial Emissions Containing
595 O2, H2O and SO2: Behavior of Fe/ZSM-5 Catalysts, Catal. Today. 53 (1999) 683–693.
596 doi:10.1016/S0920-5861(99)00155-8.

597 [49] H. Abdulhamid, E. Fridell, M. Skoglundh, Influence of the Type of Reducing Agent (H 2 , CO, C 3
598 H 6 and C 3 H 8) on the Reduction of Stored NO X in a Pt/BaO/Al 2 O 3 Model Catalyst, Top.
599 Catal. 30/31 (2004) 161–168. doi:10.1023/B:TOCA.0000029745.87107.b8.

600 [50] G. Djéga-Mariadassou, F. Fajardie, J.F. Tempère, J.M. Manoli, O. Touret, G. Blanchard, A general
601 model for both three-way and deNO(x) catalysis: Dissociative or associative nitric oxide
602 adsorption, and its assisted decomposition in the presence of a reductant. Part I. Nitric oxide
603 decomposition assisted by CO over reduced or oxidized rhodiu, J. Mol. Catal. A Chem. 161
604 (2000) 179–189. doi:10.1016/S1381-1169(00)00334-4.

605 [51] L. He, L.C. Wang, H. Sun, J. Ni, Y. Cao, Y. He, K.N. Fan, Efficient and selective room-temperature
606 gold-catalyzed reduction of nitro compounds with CO and H2O as the hydrogen source, Angew.
607 Chemie - Int. Ed. 48 (2009) 9538–9541. doi:10.1002/anie.200904647.

608 [52] K. Teramura, T. Tanaka, H. Ishikawa, Y. Kohno, T. Funabiki, Photocatalytic Reduction of CO_2 to
609 CO in the Presence of H_2 or CH_4 as a Reductant over MgO, J. Phys. Chem. B. 108 (2004) 346–
610 354. doi:10.1021/jp0362943.

611 [53] K. Yogo, M. Ihara, I. Terasaki, E. Kikuchi, Selective Reduction of Nitrogen Monoxide with
612 Methane or Ethane on Gallium Ion-exchanged ZSM-5 in Oxygen-rich Atmosphere, Chem. Lett.
613 22 (1993) 229–232. doi:10.1246/cl.1993.229.

614 [54] R. Burch, P.K. Loader, Investigation of Pt /& Q , and Pd / A & catalysts for the combustion of
615 methane at low concentrations, Appl. Catal. B Environ. 5 (1994) 149–164.

616 [55] M. Konsolakis, I. V. Yentekakis, G. Pekridis, N. Kaklidis, A.C. Psarras, G.E. Marnellos, Insights
617 into the role of SO2 and H2O on the surface characteristics and de-N2O efficiency of Pd/Al2O3
618 catalysts during N2O decomposition in the presence of CH4 and O2 excess, Appl. Catal. B
619 Environ. 138–139 (2013) 191–198. doi:10.1016/j.apcatb.2013.02.038.

620 [56] V.K. Tzitzios, V. Georgakilas, Catalytic reduction of N2O over Ag-Pd/Al2O3bimetallic catalysts,
621 Chemosphere. 59 (2005) 887–891. doi:10.1016/j.chemosphere.2004.11.021.

622 [57] E. Pachatouridou, E. Papista, E.F. Iliopoulou, A. Delimitis, G. Goula, I.V. Yentekakis, G.E.
623 Marnellos, M. Konsolakis, Nitrous oxide decomposition over Al2O3 supported noble metals (Pt,
624 Pd, Ir): Effect of metal loading and feed composition, J. Environ. Chem. Eng. 3 (2015) 815–821.
625 doi:10.1016/j.jece.2015.03.030.

626 [58] M. Morad, M. Sankar, E. Cao, E. Nowicka, T.E. Davies, P.J. Miedziak, D.J. Morgan, D.W. Knight,
627 D. Bethell, A. Gavriilidis, G.J. Hutchings, Solvent-free aerobic oxidation of alcohols using
628 supported gold palladium nanoalloys prepared by a modified impregnation method, Catal. Sci.
629 Technol. 4 (2014) 3120–3128. doi:10.1039/C4CY00387J.

630 [59] F. Hu, X. Wu, Y. Wang, X. Lai, Ultrathin γ-Al2O3 nanofibers with large specific surface area and
631 their enhanced thermal stability by Si-doping, RSC Adv. 5 (2015) 54053–54058.
632 doi:10.1039/C5RA08315J.

[60] B. Ngamsom, N. Bogdanchikova, M.A. Borja, P. Praserthdam, Characterisations of Pd-Ag/Al2O3 catalysts for selective acetylene hydrogenation: Effect of pretreatment with NO and N 2O, Catal. Commun. 5 (2004) 243–248. doi:10.1016/j.catcom.2004.02.007.

[61] Y. Ning, Z. Yang, H. Zhao, Platinum recovery by palladium alloy catchment gauzes in nitric acid plants: The mechanism of platinum recovery, Platin. Met. Rev. 40 (1996) 80–87.

[62] P. Marécot, A. Fakche, B. Kellali, G. Mabilon, P. Prigent, J. Barbier, Propane and propene oxidation over platinum and palladium on alumina: Effects of chloride and water, Applied Catal. B, Environ. 3 (1994) 283–294. doi:10.1016/0926-3373(94)00003-4.

[63] J. Batista, A. Pintar, D. Mandrino, M. Jenko, V. Martin, XPS and TPR examinations of ??-alumina-supported Pd-Cu catalysts, Appl. Catal. A Gen. 206 (2001) 113–124. doi:10.1016/S0926-860X(00)00589-5.

[64] J.Z. Shyu, K. Otto, W.L.H. Watkins, G.W. Graham, R.K. Belitz, H.S. Gandhi, Characterization of Pd/??-alumina catalysts containing ceria, J. Catal. 114 (1988) 23–33. doi:10.1016/0021-9517(88)90005-X.

[65] L. Liu, F. Zhou, L. Wang, X. Qi, F. Shi, Y. Deng, Low-temperature CO oxidation over supported Pt, Pd catalysts: Particular role of FeOx support for oxygen supply during reactions, J. Catal. 274 (2010) 1–10. doi:10.1016/j.jcat.2010.05.022.

[66] A. Tressaud, S. Khairoun, H. Touhara, N. Watanabe, X-Ray Photoelectron Spectroscopy of Palladium Fluorides, Zeitschrift Anorg. Und Allg. Chemie. 540 (1986) 291–299. doi:10.1002/zaac.19865400932.

[67] J.C. Zhou, C.M. Soto, M.-S. Chen, M.A. Bruckman, M.H. Moore, E. Barry, B.R. Ratna, P.E. Pehrsson, B.R. Spies, T.S. Confer, Biotemplating rod-like viruses for the synthesis of copper nanorods and nanowires, J. Nanobiotechnol. 10 (2012) 18. doi:10.1186/1477-3155-10-18.

[68] M.C. Militello, S.J. Simko, Palladium Chloride (PdCl 2) by XPS INSTRUMENT PARAMETERS COMMON TO ALL, Surf. Sci. 3 (1997) 402–409.

[69] R.J. Liu, P.A. Crozier, C.M. Smith, D.A. Hucul, J. Blackson, G. Salaita, Metal sintering mechanisms and regeneration of palladium/alumina hydrogenation catalysts, Appl. Catal. A Gen. 282 (2005) 111–121. doi:10.1016/j.apcata.2004.12.015.

[70] J.J. Chen, E. Ruckenstein, Sintering of palladium on alumina model catalyst in a hydrogen atmosphere, J. Catal. 69 (1981) 254–273. doi:10.1016/0021-9517(81)90163-9.

[71] W. Chen, Y. Ding, X. Song, T. Wang, H. Luo, Promotion effect of support calcination on ethanol production from CO hydrogenation over Rh/Fe/Al2O3catalysts, Appl. Catal. A Gen. 407 (2011) 231–237. doi:10.1016/j.apcata.2011.08.044.

[72] N. Yao, J. Chen, J. Zhang, J. Zhang, Influence of support calcination temperature on properties of Ni/TiO2for catalytic hydrogenation of o-chloronitrobenzene to o-chloroaniline, Catal. Commun. 9 (2008) 1510–1516. doi:10.1016/j.catcom.2007.12.022.

[73] C.E. Bronnimann, I. ssuer Chuang, B.L. Hawkins, G.E. Maciel, Dehydration of Silica—Aluminas Monitored by High-Resolution Solid-State Proton NMR, J. Am. Chem. Soc. 109 (1987) 1562–1564. doi:10.1021/ja00239a043.

[74] E.C. Decanio, J.C. Edwards, J.W. Bruno, Solid-State 1H MAS NMR Characterization of [gamma]-Alumina and Modified [gamma]-Aluminas, J. Catal. 148 (1994) 76–83. doi:10.1006/jcat.1994.1187.

[75] M. Hunger, D. Freude, H. Pfeifer, H. Bremer, M. Jank, K.P. Wendlandt, High-resolution proton

magnetic resonance and catalytic studies concerning brønsted centers of amorphous Al2O3-SiO2 solids, Chem. Phys. Lett. 100 (1983) 29–33. doi:10.1016/0009-2614(83)87256-X.

[76] J. Park, J.R. Regalbuto, A Simple, Accurate Determination of Oxide PZC and the Strong Buffering Effect of Oxide Surfaces at Incipient Wetness, J. Colloid Interf. Sci. 175 (1995) 239–252. doi:10.1006/jcis.1995.1452.

[77] K.P. De Jong, Synthesis of Solid Catalysts, 1st ed., Wiley-VCH Verlag GmbH & Co. KGaA, 2009.

[78] P. Munnik, P.E. De Jongh, K.P. De Jong, Recent Developments in the Synthesis of Supported Catalysts, Chem. Rev. 115 (2015) 6687–6718. doi:10.1021/cr500486u.